SAND2005-7390C

**Laser-induced incandescence of flame-generated soot on a picosecond timescale**

Hope A. Michelsen

Combustion Research Facility

Sandia National Laboratories

P. O. Box 969

MS 9055

Livermore, CA 94551

FAX: 925-294-2276

Email: hamiche@ca.sandia.gov

Colloquium: Diagnostics

Total length of paper determined by method 1: 5731

Length of main text: 2925 words

Length of references: 996 words

Equivalent length of Figure 1 and caption: 340

Equivalent length of Figure 2 and caption: 175

Equivalent length of Figure 3 and caption: 710

Equivalent length of Figure 4 and caption: 380

Equivalent length of Figure 5 and caption: 205

**Abstract**

This paper presents measurements of time-resolved laser-induced incandescence (LII) from soot recorded on a picosecond timescale. The second harmonic (532 nm) from a picosecond Nd:YAG laser was used to heat the soot, and a streak camera was used to record the LII signal. The results are compared with a model and with data collected on a nanosecond timescale. Relative to the laser timing, the picosecond and nanosecond results are very similar. Signals increase during the laser pulse as soot temperatures increase and decrease after the laser pulse. The signal decay rates increase significantly with increasing laser fluence. The LII model gives good agreement with the nanosecond data at fluences $\leq$0.2 J/cm$^2$ and underpredicts the signal decay rates at higher fluences. The picosecond temporal profiles increase significantly faster and earlier in the laser pulse than predicted by the model. This disagreement between the model and picosecond LII data is hypothesized to be attributable to perturbations to the signal by laser-induced fluorescence from polycyclic aromatic hydrocarbons or other class of large organic species that fluoresces to the red of 633 nm at high temperatures. The excited state or states responsible for this fluorescence appear to be accessed via a two-photon transition and have an effective lifetime of 55 ps.

Keywords: LII, soot, PAH, LIF, flame

## 1. Introduction

Over the past several decades laser-induced incandescence (LII) of soot has gained widespread use as a sensitive optical technique for measurements of soot volume fraction and primary particle size.[1] This technique involves heating the soot particles with a high-power pulsed laser to temperatures (2500-4000 K) at which they incandesce and measuring the emitted light. Interpretation of LII signals for quantitative measurements is hampered by an incomplete understanding of the microphysical mechanisms that influence signal evolution during and after the laser pulse. Previous experimental work has shown that, at low fluences (<~0.15 J/cm$^2$), temporally resolved LII signals increase during the laser pulse and slowly decay with decay times on the order of a few hundred nanoseconds.[2-7] Decay times decrease with increasing fluence, particularly at fluences above 0.2 J/cm$^2$.[2, 3, 5, 6, 8-10] These previous studies have been performed using laser systems with pulse durations in the range of 7-8 ns. In the work presented here, a picosecond laser was used to heat the soot, and a streak camera was used to collect the signal. These experiments were performed to gain a better understanding of the relatively fast physical and chemical processes that can influence the LII signal.

## 2. Experimental setup

A schematic diagram of the experimental setup is shown in Fig. 1. Soot was generated in a nonsmoking laminar diffusion flame at atmospheric pressure. The burner with which it was produced is commonly referred to as a Santoro burner and has a brass fuel tube with a 1.1 cm inner diameter surrounded by ceramic honeycomb with a 10.2 cm outer diameter for the co-flow of air.[11-18] The flame was stabilized with a chimney 19.5 cm tall and 10.2 cm in diameter. Mass flow controllers (MKS types 1479A for low

flow and 1559A for high flow) were used to maintain flow rates in the range of 0.23 standard liters per minute (SLM) ethylene for the fuel and 64 SLM for the air. The visible flame height for these conditions was 9.8 cm. Measurements were made at a height of 5 cm above the burner on the front edge of the flame to avoid (1) laser attenuation in the flame and (2) re-absorption of LII between the detection region in the flame and the detector.

The laser light for the picosecond experiments was generated by a regeneratively amplified modelocked Nd:YAG laser (Positive Light RGN-A with a Time-Bandwidth Products GE-100 seeder), which produced temporally smooth pulses at a wavelength of 532 nm and a repetition rate of 20 Hz with a duration of 65 ps FWHM and a beam diameter of ~0.79 cm. For the nanosecond experiments the laser light was produced by an injection-seeded Nd:YAG laser (Spectra-Physics GCR5 with a Quanta-Ray 6300 seeder). This laser generated 532-nm pulses with a smooth temporal profile, duration of 6.9 ns FWHM, repetition rate of 10 Hz, and beam diameter of ~0.79 cm. The optical setup was the same for both experiments. A ceramic aperture with a diameter of 0.315 cm was placed at the output of the laser to select the central portion of the beam. The aperture was relay imaged to the detection region in the flame using a telescope with a 100-cm lens followed by a 50-cm lens, the combination of which reduced the beam size by a factor of two. A beam profiler with 8.4 X 9.8 μm pixel size (Coherent Digital BeamView Analyzer) was used to monitor the spatial profile produced at the flame by this optical configuration (see Fig. 2). The beam was attenuated with a half-wave plate followed by two thin-film polarizers, and the fluence was monitored using a surface-

absorbing thermal detector (Molectron PM10). The beam profiles were independent of fluence.

For the picosecond experiments the LII signal and laser light elastically scattered from the soot were imaged with two 6-cm spherical achromatic lenses onto the slit of a streak camera (Hamamatsu C2830) coupled to a CCD camera (Photometrics CH350). The LII and scattered light were simultaneously collected on each laser shot with a temporal resolution of ~8 ps. The LII signal was collected on one side of the slit through a 633-nm dichroic edge filter (Semrock RazorEdge) and two 0.3-cm long-pass colored-glass filters (Schott RG 610), and the elastic scatter was collected on the other side of the slit through a 532-nm bandpass filter (Semrock MaxLine) and a selection of absorptive neutral density filters. Dichroic filters were used in front of the colored-glass filters to avoid fluorescence from the colored-glass filters. Two hundred laser shots were averaged for each temporal profile presented. Measurements were made over the entire edge of the flame, which corresponded to a radial position of 0.23±0.11 cm.

For the nanosecond experiments the LII was similarly imaged through a 0.3-cm long-pass colored-glass filter (Corning RG610) onto a fast silicon photodiode (Electro-Optics Technology ET-2030) with a rise time of <300 ps and an active area of 0.04-cm diameter. The signal was recorded on an oscilloscope with a 3-GHz bandwidth (Tektronics TDS694C), which was triggered by another fast silicon photodiode viewing 532-nm light leaking through the first dichroic mirror, i.e., prior to the half-wave plate used for attenuation. LII temporal profiles were recorded on a timescale of 5 ns/div (10 GS/s) at fluences between 0.01 and 3.71 J/cm$^2$. Measurements were made at a radial position of

0.23±0.02 cm from the center of the flame, which is the region of highest soot volume fraction.[12] Two hundred laser shots were averaged for each temporal profile presented.

## 3. Model description

The LII model presented here has been described in detail elsewhere.[5] It solves the energy- and mass-balance equations to account for particle heating by laser absorption, annealing, and oxidation and cooling by conduction to the surrounding atmosphere, radiative emission, sublimation, and non-thermal photodesorption of carbon clusters $C_2$ and $C_3$. Particle-size reduction during sublimation, photodesorption, and oxidation is also calculated. The model includes (1) temperature-dependent thermodynamic parameters for calculating sublimation, conduction, and internal energy storage by the particle; (2) wavelength-dependent optical parameters to describe absorption and emission of radiation based on a Rayleigh-Debye-Gans (RDG) approximation to account for aggregation; (3) convective heat and mass flow (Stefan flow) during the sublimation of multiple cluster species (C, $C_2$, $C_3$, $C_4$, and $C_5$) from the surface; (4) a thermal accommodation coefficient appropriate for high-temperature conductive cooling; (5) a conductive cooling mechanism assuming free molecular flow at low pressure and a transition regime at high pressure; and (6) the effects of annealing on absorption, radiation, sublimation, and photodesorption.

The model descriptions of cooling and mass loss by sublimation and photodesorption are the most important components of the model for calculating particle size and temperature at fluences above 0.2 J/cm$^2$. This part of the model is also the most complex and, in the case of photodesorption, the most uncertain. Although previous studies suggested that laser photodesorption of carbon clusters from graphite can proceed by a

nonthermal mechanism,[19-24] the nature of this mechanism, including the number of photons required, is not known. Our model includes such a mechanism, assuming that it proceeds via a two-photon process at 532 nm with a cross section and enthalpy of reaction approximated by comparing the results with data taken previously using a system similar to that described above for the nanosecond experiment.[6] Annealing rates are calculated using an Arrhenius expression, with activation energies for interstitial migration and vacancy/defect formation derived from studies of graphitization.

All calculations are for a single primary particle and assume minimal contact between primary particles in an aggregate. Aggregation is expected to decrease conductive cooling rates via the shielding effect.[25-27] Quasi-Monte-Carlo simulations indicate that accounting for aggregation reduces the conductive cooling rate by ~30% for an aggregate of 500 primary particles,[25] and will have less of effect for the aggregates considered here for which the number of primary particles per aggregate was much smaller.[13, 15] The mean aggregate size was ~100 nm with a primary particle diameter of ~32 nm.[13, 14] Aggregation also influences the particle optical properties, but these are accounted for by the use a RDG approximation for absorption and emission. The temperature was assumed to be 1800 K.[12]

**4. Results and discussion**

The temporal behavior of the LII signal during and after picosecond laser pulses is remarkably similar to that observed during and after nanosecond laser pulses. The picosecond and nanosecond results are shown for comparison in Fig. 3. At all fluences signals increase during the laser pulse as soot absorbs light and becomes hot enough to emit detectable incandescence. Decay rates are slower at the lower fluences and increase

with increasing fluence, such that the LII peak becomes narrower with fluence. At the low fluences (<0.1 J/cm$^2$) the rate of decay of the signal is predominantly determined by the conductive cooling rate of the particle. Because the LII signal is approximately proportional to $T^5$, particle cooling leads to a decrease in signal. LII signals also depend on particle size and decrease approximately linearly with a decrease in particle volume. Thus, at higher fluences (≥ 0.2 J/cm$^2$) cooling and mass loss by sublimation and possibly photodesorption lead to significantly larger initial signal decay rates.

The LII model qualitatively reproduces this slow decay in signal at low fluences and faster decay at high fluences for both picosecond and nanosecond experiments. Quantitatively it gives good agreement with the nanosecond data at low fluences (≤ 0.2 J/cm$^2$) but does not decay rapidly enough at higher fluences. These results have been discussed in detail previously.[5, 6] The overall agreement between the data and the model for the picosecond experiments is not as good. At all fluences the measured signal starts to increase earlier in the laser pulse and decays faster after the laser pulse than predicted by the model.

There are other noteworthy differences between the picosecond and nanosecond temporal behavior not captured by the model. For the nanosecond experiment the rising edge of the signal during the laser pulse becomes much steeper with increasing fluence. This change in the rising edge of the temporal profiles is not obvious for the picosecond experiment. Over the range of fluences shown in Fig. 3, the rate of signal growth increases by a factor of ~4.5 in the nanosecond experiment but only by ~30% in the picosecond experiment. This increase in signal growth rate with fluence is reproduced in

model calculations for the nanosecond experiment (see Fig. 3). The increase predicted for the picosecond experiment (a factor of ~2.3) is much larger than observed.

The mechanism that controls the onset and rise time of the signal in the model is the absorptive heating rate. One potential explanation for a late signal onset is an underestimation of the absorption cross section. Increasing the absorption cross section moves the LII onset to earlier times. In order to reproduce the signal onset at the lower fluences, the absorption cross section would have to be approximately an order of magnitude larger than the current value, which is not consistent with previous measurements.[28-31] Such an increase in the absorption cross section would also substantially increase the decay rate and the rise time, which is inconsistent with the temporal behavior shown in Fig. 3.

An alternative explanation for the early signal onset involves contributions from a source other than soot. One potential source of interference is laser-induced fluorescence (LIF) from polycyclic aromatic hydrocarbons (PAHs). PAHs are precursors to soot formation and are abundant in regions of flames where soot inception occurs.[16, 17, 32, 33] At high temperatures laser excitation of PAHs at visible and UV wavelengths produces broadband, featureless fluorescence from states with short lifetimes (in the range of picoseconds to nanoseconds).[34-41] Such broadband fluorescence observed in flames has been attributed to PAH LIF and has been used to measure PAH distributions.[18, 42-53] Previous work using a nanosecond laser system indicated that fluorescence from PAHs induced by 532-nm laser excitation should be insignificant in the region of the flame in which the measurements were made (i.e., at a height of 5 cm above the burner).[18, 47, 48] The good agreement between the modeled and measured

LII shown in Fig. 3 also suggests that PAH LIF does not significantly perturb the measured nanosecond temporal profiles presented here.

It is possible that the model adequately predicts the LII temporal behavior and that the fast interference feature only perturbs the initial part of the measured temporal profile. Figure 4 shows the modeled curve scaled to the measured curve between 1 and 3 ns. Assuming that the model reproduces the LII behavior after the laser pulse, subtracting the modeled temporal profile from the measured profile provides information about the interference. The difference between the modeled and measured curves is shown in Fig. 4. Within the temporal uncertainty of the experiment the timing of the resulting peak is independent of fluence. Between 0.050 and 0.525 J/cm$^2$ the peak occurs at 15±8 ps after the peak of the laser pulse. This timing is consistent with fluorescence from a short-lived excited state of a gas-phase species interacting with the 532-nm laser beam. An exponential fit to the falling edge of this peak yields a value for the decay time of 55 ps with a random error of less than 1%. Figure 4 shows the integrated intensity of this peak plotted as a function of laser fluence. The peak intensity varies approximately quadratically with laser fluence, suggesting that the excited state is accessed via a two-photon process. Such a state will likely be more readily accessible with a picosecond laser pulse than with a nanosecond laser pulse, which could explain why the picosecond temporal profiles are perturbed by this interference whereas the nanosecond results are not.

Previous studies have shown that single-photon excitation of small PAHs at 266 nm (i.e., the energetic equivalent of two 532-nm photons) results in fluorescence in the range of 300-450 nm at room temperature and that the fluorescence is shifted to longer

wavelengths (as long as 600 nm) at elevated temperatures.[37, 38] Although these wavelengths are shorter than those detected in the present experiment (>633 nm), these broad fluorescence bands can have long-wavelength tails extending into our detection regime. Lifetimes of the excited states involved in this fluorescence have been measured to be in the range of 160 ns at room temperature.[54] Lifetimes decrease with increasing temperature[37, 38, 54, 55] and have been measured in the range of 0.2-30 ns at 1000-1600 K.[37, 38] Presumably these lifetimes could be even shorter at temperatures near 1800 K, which are relevant to the present experiment.

These previous studies neither preclude identification of the interference as PAH LIF nor provide a definitive identification. Because PAH concentrations are relatively high in sooty flames, PAHs are a likely candidate for such interferences. It is possible, however, that results from the present experiment are perturbed by LIF from another class of large organic species. Future work will involve recording temporal profiles at other locations in the flame. At lower heights in the flame PAH concentrations are higher, and optical signatures from PAHs should be enhanced. Similar experiments will also be performed at 1064 nm for which interferences from LIF from gas-phase species should be less significant.

## 5. Conclusions

This paper presents measurements of time-resolved LII from soot recorded on a picosecond timescale. Soot was produced in an atmospheric laminar co-flow diffusion burner and was heated with the 532-nm output from a picosecond Nd:YAG laser with a pulse duration of 65 ps. The signal was recorded on a streak camera with a temporal resolution of ~8 ps. Similar measurements were made using the 532-nm output from a

Nd:YAG with a 6.9-ns pulse duration to heat the soot and a photodiode with a rise time of <0.3 ns to record the signal. Relative to the laser timing, the temporal characteristics of the picosecond and nanosecond signals are qualitatively very similar. Signals increase during the laser pulse as soot temperatures increase and decrease after the laser pulse. The signal decay rates increase significantly with increasing laser fluence.

The results of both experiments were compared with an LII model that has been optimized using data from a nanosecond LII system. As has been demonstrated previously,[5, 6] the LII model gives good agreement with the nanosecond data at fluences $\leq$0.2 J/cm$^2$ and under-predicts the signal decay rates at higher fluences. The model does not agree as well with the picosecond data. The picosecond temporal profiles increase significantly faster and earlier in the laser pulse than predicted by the model. This disagreement between the model and picosecond LII data may be attributable to perturbations to the signal by LIF from PAHs or other class of large organic species that fluoresces in the range of 633-900 nm. The power dependence of the signal enhancement suggests that the excited state or states responsible for this fluorescence are accessed via a two-photon transition, which would explain the enhanced sensitivity to this interference with the shorter pulse duration. These states are short-lived and are estimated to have an effective lifetime of ~55 ps.

**Acknowledgements**

I am grateful to Tom Settersten for sharing his insight, knowledge, and enthusiasm with me. I thank Brian Patterson for his help keeping the picosecond laser system running and Engelene Chrysostom, Roger Farrow, and Paul Schrader for assistance with the initial setup of this experiment. This work was supported by the Division of

Chemical Sciences, Geosciences, and Biosciences, the Office of Basic Energy Sciences, the U. S. Department of Energy. Sandia is a multi-program laboratory operated by Sandia Corporation, a Lockheed Martin Company, for the National Nuclear Security Administration under contract DE-AC04-94-AL85000.

**References**

[1] R.J. Santoro, C.R. Shaddix, *Laser-Induced Incandescence*, in *Applied Combustion Diagnostics*, K. Kohse-Höinghaus and J.B. Jeffries, Editors. 2002, Taylor & Francis: New York, NY. p. 252-286.

[2] T. Ni, J.A. Pinson, S. Gupta, R.J. Santoro, *Appl. Opt.* 34 (1995) 7083-7091.

[3] P.O. Witze, S. Hochgreb, D. Kayes, H.A. Michelsen, C.R. Shaddix, *Appl. Opt.* 40 (2001) 2443-2452.

[4] T. Schittkowski, B. Mewes, D. Brüggemann, *Phys. Chem. Chem. Phys.* 4 (2002) 2063-2071.

[5] H.A. Michelsen, *J. Chem. Phys.* 118 (15) (2003) 7012-7045.

[6] H.A. Michelsen, P.O. Witze, D. Kayes, S. Hochgreb, *Appl. Opt.* 42 (27) (2003) 5577-5590.

[7] D.R. Snelling, F. Liu, G.J. Smallwood, Ö.L. Gülder, *Combust. Flame* 136 (2004) 180-190.

[8] R.L. Vander Wal, K.J. Weiland, *Appl. Phys. B* 59 (1994) 445-452.

[9] A.V. Filippov, M.W. Markus, P. Roth, *J. Aerosol Sci.* 30 (1999) 71-87.

[10] C. Allouis, F. Beretta, A. D'Alessio, *Exp. Thermal Fluid Sci.* 27 (2003) 455-463.

[11] R.J. Santoro, H.G. Semerjian, R.A. Dobbins, *Combust. Flame* 51 (1983) 203-218.

[12] R.J. Santoro, J.H. Miller, *Langmuir* 3 (1987) 244-254.

[13] R.A. Dobbins, C.M. Megaridis, *Langmuir* 3 (1987) 254-259.

[14] Ü.Ö. Köylü, C.S. McEnally, D.E. Rosner, L.D. Pfefferle, *Combust. Flame* 110 (1997) 494-507.

[15] R.A. Fletcher, R.A. Dobbins, H.-C. Chang, *Anal. Chem.* 70 (13) (1998) 2745-2749.

[16] K. Siegmann, K. Sattler, H.C. Siegmann, *J. Electron Spectrosc. Relat. Phenom.* 126 (2002) 191-202.

[17] H. Hepp, K. Siegmann, *Combust. Flame* 115 (1998) 275-283.

[18] K.C. Smyth, C.R. Shaddix, D.A. Everest, *Combust. Flame* 111 (1997) 185-207.

[19] D.J. Krajnovich, *J. Chem. Phys.* 102 (1995) 726-743.

[20] K.A. Lincoln, M.A. Covington, *Int. J. Mass Spectrom. Ion Phys.* 16 (1975) 191-208.

[21] R.W. Dreyfus, R. Kelly, R.E. Walkup, *Nucl. Instrum. Methods Phys. Res.* B23 (1987) 557-561.

[22] P.T. Murray, D.T. Peeler, *Appl. Surf. Sci.* 69 (1993) 225-230.

[23] F. Kokai, K. Takahashi, M. Yudasaka, S. Iijima, *J. Phys. Chem. B* 103 (1999) 8686-8693.

[24] E.A. Rohlfing, *J. Chem. Phys.* 89 (1988) 6103-6112.

[25] A.V. Filippov, M. Zurita, D.E. Rosner, *J. Colloid Interface Sci.* 229 (2000) 261-273.

[26] D.R. Snelling, F. Liu, G.J. Smallwood, Ö.L. Gülder, *Combust. Flame* 136 (2002) 180-190.

[27] F. Liu, G.J. Smallwood, D.R. Snelling, *J. Quant. Spectrosc. Radiat. Transfer* 93 (2005) 301-312.

[28] H. Chang, T.T. Charalampopoulos, *Proc. R. Soc. London, A* 430 (1990) 577-591.

[29] K.C. Smyth, C.R. Shaddix, *Combust. Flame* 107 (1996) 314-320.

[30] Ü.Ö. Köylü, G.M. Faeth, *J. Heat Transfer* 118 (1996) 415-421.

[31] Ü.Ö. Köylü, *Combust. Flame* 109 (1996) 488-500.

[32] T. Baum, P. Löffler, P. Weilmünster, K.-H. Homann, *Ber. Bunsen-Ges. Phys. Chem.* 96 (7) (1992) 841-857.

[33] H. Richter, J.B. Howard, *Prog. Energy Combust. Sci.* 26 (2000) 565-608.

[34] D.S. Coe, J.I. Steinfeld, *Chem. Phys. Lett.* 76 (3) (1980) 485-489.

[35] D.S. Coe, B.S. Haynes, J.I. Steinfeld, *Combust. Flame* 43 (1981) 211-214.

[36] A. Thöny, M.J. Rossi, *J. Photochem. Photobiol., A* 104 (1997) 25-33.

[37] F. Ossler, T. Metz, M. Aldén, *Appl. Phys. B* 72 (2001) 479-489.

[38] F. Ossler, T. Metz, M. Aldén, *Appl. Phys. B* 72 (2001) 465-478.

[39] L.R. Allain, D.N. Stratis, B.M. Cullum, J. Mobley, M.R. Hajaligol, T. Vo-Dinh, *J. Anal. Appl. Pyrolysis* 66 (2003) 145-154.

[40] Z. Chi, B.M. Cullum, D.L. Stokes, J. Mobley, G.H. Miller, M.R. Hajaligol, T. Vo-Dinh, *Spectrochim. Acta, Part A* 57 (2001) 1377-1384.

[41] A. Leipertz, F. Ossler, M. Aldén, *Polycyclic Aromatic Hydrocarbons and Soot Diagnostics by Optical Techniques*, in *Applied Combustion Diagnostics*, K. Kohse-Höinghaus and J.B. Jeffries, Editors. 2002, Taylor & Francis: New York, NY. p. 359-383.

[42] A. Di Lorenzo, A. D'Alessio, V. Cincotti, S. Masi, P. Menna, C. Venitozzi, *Proc. Combust. Inst.* 18 (1981) 485-491.

[43] P. Andreussi, B. Barbieri, L. Petarca, *Combust. Sci. Technol.* 49 (1986) 123-141.

[44] A. Gomez, M.G. Littman, I. Glassman, *Combust. Flame* 70 (1987) 225-241.

[45] L. Petarca, F. Marconi, *Combust. Flame* 78 (1989) 308-325.

[46] F. Cignoli, S. Benecchi, G. Zizak, *Opt. Lett.* 17 (4) (1992) 229-231.

[47] R.L. Vander Wal, K.A. Jensen, M.Y. Choi, *Combust. Flame* 109 (1997) 399-414.

[48] R.L. Vander Wal, *Combust. Flame* 112 (1998) 607-616.

[49] C.S. McEnally, L.D. Pfefferle, *Combust. Flame* 121 (2000) 575-592.

[50] A. Ciajolo, R. Ragucci, B. Apicella, R. Barbella, M. de Joannon, A. Tregrossi, *Chemosphere* 42 (2001) 835-841.

[51] A. Ciajolo, B. Apicella, R. Barbella, A. Tregrossi, F. Beretta, C. Allouis, *Energy Fuels* 15 (2001) 987-995.

[52] A. Ciajolo, A. Tregrossi, R. Barbella, R. Ragucci, B. Apicella, M. de Joannon, *Combust. Flame* 125 (2001) 1225-1229.

[53] C.R. Shaddix, T.C. Williams, L.G. Blevins, R.W. Shefer, *Proc. Combust. Inst.* 30 (2005) 1501-1508.

[54] T. Ni, L.A. Melton, *Appl. Spectrosc.* 50 (9) (1996) 1112-1116.

[55] T. Deinum, C.J. Werkhoven, J. Langelaar, R.P.H. Rettschnick, J.D.W. van Voorst, *Chem. Phys. Lett.* 27 (2) (1974) 206-209.

**Figure captions**

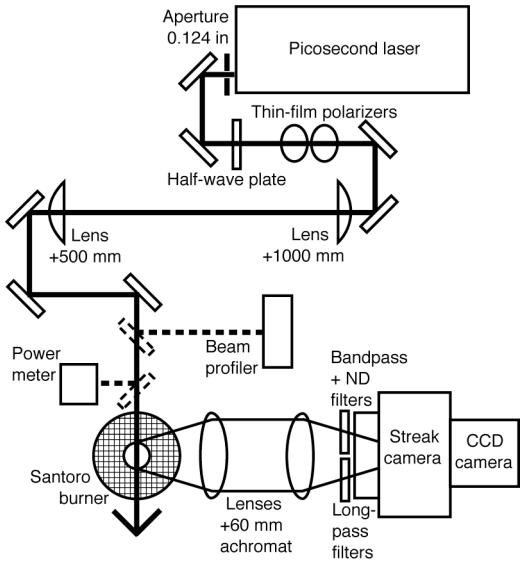


Figure 1. Experimental setup. Soot was generated in an ethylene/air nonsmoking laminar flame from a co-flow diffusion burner at atmospheric pressure. The central portion of the laser beam produced by a picosecond laser was relay imaged with a 2:1 telescope into the detection region at the flame. A beam profiler was used to monitor the spatial profile produced at the flame by this optical configuration. The beam was attenuated with a half-wave plate followed by two thin-film polarizers, and the fluence was monitored using a surface-absorbing thermal detector. The LII signal and laser light elastically scattered from the soot were imaged onto the slit of a streak camera and simultaneously collected on each laser shot. The LII signal was collected on one side of the slit through a combination of long-pass filters, and the laser scatter was collected on the other side of the slit through a combination of 532-nm bandpass and neutral density filters.

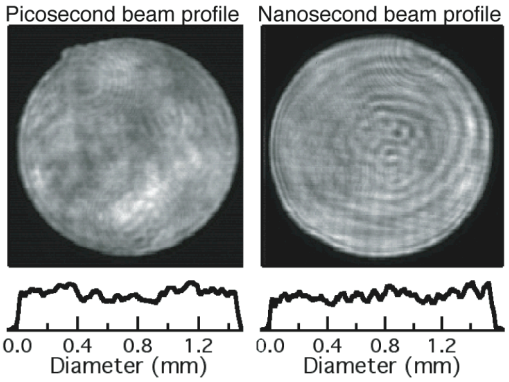


Figure 2. Laser beam spatial profiles at the flame. The spatial profiles are shown with cross-sectional cuts through the profile centers. The 1-σ standard deviation from the mean over a single-shot profile was ±20% for the picosecond experiment and ±16% for the nanosecond experiment.

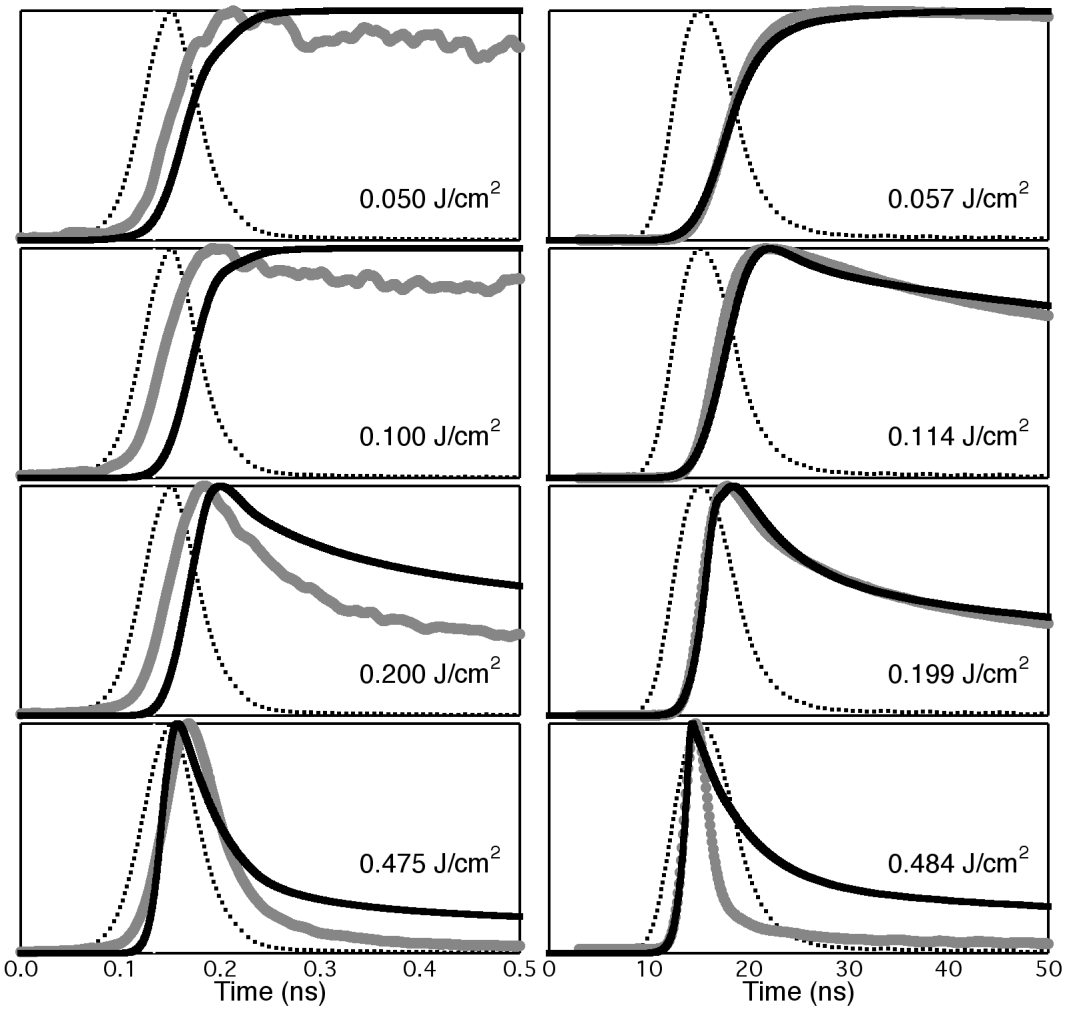


Figure 3. LII temporal profiles from the picosecond and nanosecond experiments. The left panels show results from the picosecond experiment at four fluences, and the right panels present results from the nanosecond experiment at similar fluences. The dotted line in each panel is the laser temporal profile. The gray symbols represent the data points from 200 averaged profiles. The solid black line is the modeled LII profile. The peak of each curve has been scaled to the top of the graph.

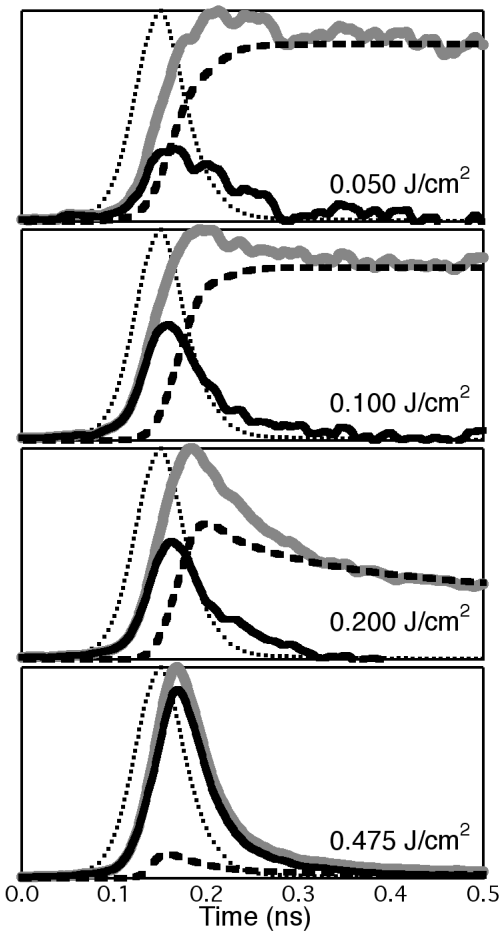


Figure 4. Analysis of the picosecond temporal profiles. The measured (gray symbols) and modeled (dashed black lines) temporal profiles are the same as those shown for the picosecond experiment in Fig. 3. The modeled LII curves have been rescaled such that the mean of the modeled profile in the time range of 1-3 ns equals the mean of the measured profile in the same time range. The dotted line in each panel is the laser temporal profile. The solid black line is the difference between the measured and modeled profiles.

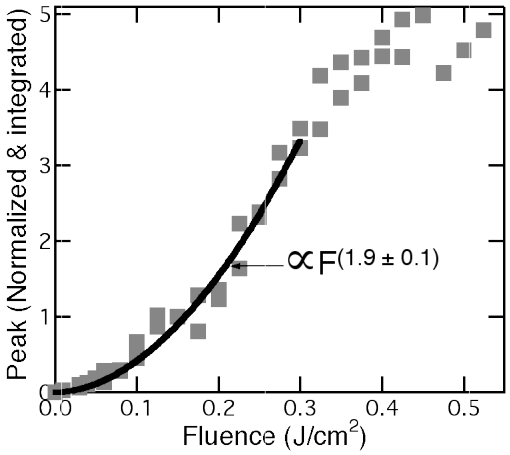


Figure 5. Power-dependence of the interference peak. The symbols represent the results of integrating the peak inferred from the difference between the measured and modeled temporal profiles (e.g., solid black curves in Fig. 4). The line presents the results of a power-law fit to the symbols for fluences less than or equal to 0.3 J/cm$^2$.